bioRxiv preprint doi: https://doi.org/10.1101/431650; this version posted October 1, 2018. The copyright holder for this preprint (which was not certified by peer review) is the author/funder. All rights reserved. No reuse allowed without permission.

Redistribution of a glucuronoxylomannan epitope towards the capsule surface coincides with Titanisation in the human fungal pathogen *Cryptococcus neoformans*

Mark Probert[1], Xin Zhou[1], Margaret Goodall[2], Simon A. Johnston[3], Ewa Bielska[1], Elizabeth R. Ballou[1], Robin C. May[1]

[1]Institute of Microbiology & Infection and School of Biosciences, University of Birmingham, Edgbaston, Birmingham, UK. B15 2TT

[2]Institute of Immunology & Immunotherapy, University of Birmingham, Edgbaston, Birmingham, UK. B15 2TT

[3]Department of Infection, Immunity and Cardiovascular Disease and Bateson Centre, University of Sheffield, Sheffield, UK. S10 2TN.

Correspondence to: r.c.may@bham.ac.uk.
+44-121-4145418

bioRxiv preprint doi: https://doi.org/10.1101/431650; this version posted October 1, 2018. The copyright holder for this preprint (which was not certified by peer review) is the author/funder. All rights reserved. No reuse allowed without permission.

Abstract

Disseminated infections with the fungal species *Cryptococcus neoformans* or, less frequently, *C. gattii*, are a leading cause of mortality in immunocompromised individuals. Central to the virulence of both species is an elaborate polysaccharide capsule that consists predominantly of glucuronoxylomannan (GXM). Due to its abundance, GXM is an ideal target for host antibodies, and several monoclonal antibodies (mAbs) have previously been derived using purified GXM or whole capsular preparations as antigen. In addition to their application in the diagnosis of cryptococcosis, anti-GXM mAbs are invaluable tools for studying capsule structure. In this study, we report the production and characterisation of a novel anti-GXM mAb, Crp127, that unexpectedly reveals a role for GXM remodelling during the process of fungal Titanisation. We show that Crp127 recognises a GXM epitope in an *O*-acetylation dependent, but xylosylation-independent, manner. The epitope is differentially expressed by the four main serotypes of *Cryptococcus neoformans* and *gattii,* is heterogeneously expressed within clonal populations of *C. gattii* serotype B strains and is typically confined to the central region of the enlarged capsule. Uniquely, however, this epitope redistributes to the capsular surface in Titan cells, a recently recognised subset of giant fungal cells that are produced in the host lung and are critical for successful infection. Crp127 therefore highlights hitherto unexpected features of cryptococcal morphological change and may hold significant therapeutic potential in differentially identifying cryptococcal strains and subtypes.

Importance

Cryptococcus neoformans and *Cryptococcus gattii* are the etiological agents of cryptococcosis, an invasive fungal infection responsible for approximately 200,000 deaths each year and 15% of AIDS-related deaths annually. Whilst the main

bioRxiv preprint doi: https://doi.org/10.1101/431650; this version posted October 1, 2018. The copyright holder for this preprint (which was not certified by peer review) is the author/funder. All rights reserved. No reuse allowed without permission.

virulence factor for both species is a highly variable polysaccharide capsule, formation of Titan cells also underlies the pathogenesis of *C. neoformans.* Previous studies have shown that capsule composition differs between yeast and Titan cells, however no clear distinctions in the expression or localisation of specific capsular epitopes have been made. In this study, we characterise a novel monoclonal antibody (mAb) specific to a capsular epitope that is differentially distributed throughout the capsules produced by yeast and Titan cells. Whilst this epitope is found within the midzone of yeast capsules, the presentation of this epitope on the surface of Titan cell capsules may represent a way in which these cell types are perceived differently by the immune system.

Introduction

As the two main etiological agents of cryptococcosis, *Cryptococcus neoformans* and *Cryptococcus gattii* are major contributors to the global health burden imposed by invasive fungal infections (1). Whilst *C. neoformans* typically manifests as meningitis in immunocompromised individuals, *C. gattii* infections are not associated with specific immune defects and have been responsible for fatal outbreaks of pneumonia (2–4). Central to the virulence of both species is an elaborate polysaccharide capsule, without which *Cryptococcus* is rendered avirulent (5, 6). The composition of this capsule is highly variable and differs between yeast cells and Titan cells, the latter representing a subset of giant cells (>10 μm in cell body diameter) formed by *C. neoformans* within the host lung (7–9). Titan cells contribute to pathogenesis by resisting phagocytosis, enhancing dissemination of yeast to the central nervous system and altering host immune status (7, 9–13).

bioRxiv preprint doi: https://doi.org/10.1101/431650; this version posted October 1, 2018. The copyright holder for this preprint (which was not certified by peer review) is the author/funder. All rights reserved. No reuse allowed without permission.

The cryptococcal capsule consists of ~90% glucuronoxylomannan (GXM), ~10% glucuronoxylomannogalactan (GXMGal) and <1% mannoproteins (MPs) (14). GXM is a megadalton polysaccharide containing a backbone of α-(1,3)-mannan that is decorated with β-(1,2)-glucuronic acid, β-(1,2)-xylose and β-(1,4)-xylose substituents (15). The backbone mannan can also be *O*-acetylated, although the position at which this modification is added remains unclear for most strains (14–16). Seven repeat motifs – called structure reporter groups (SRGs) – contribute to structural variation in GXM (15). All SRGs contain a β-(1,2)-glucuronic acid on their first mannose residue, however the number of β-(1,2)- and β-(1,4)-xylose substituents varies (15). The extent and position of *O*-acetyl groups in each SRG remain unclear, however xylose and *O*-acetyl groups attached to the same mannose residue appear to be mutually exclusive (17). SRG usage differs between the four main serotypes of *Cryptococcus*, with each strain designated a serotype based on the reactivity of its capsular material with antibody preparations (18). *C. neoformans* serotypes A and D tend to biosynthesise GXM containing SRGs with fewer xylose substituents than those from *C. gattii* serotypes B and C (15, 19).

Whilst capsule structure differs between serotypes of *Cryptococcus*, a flexible biosynthetic pathway enables rapid remodelling of the capsule under different environmental conditions (20). *In vitro*, changes in *O*-acetylation have been associated with cell ageing in *C. neoformans* (21), reaffirming earlier reports that capsules produced within clonal populations are far from homogeneous (19, 22). *In vivo*, changes in capsule size and structure coincide with the infection of different organs and likely enhance fitness through the evasion of host immunity (23–25). In light of these observations, it is perhaps unsurprising that capsules produced by

bioRxiv preprint doi: https://doi.org/10.1101/431650; this version posted October 1, 2018. The copyright holder for this preprint (which was not certified by peer review) is the author/funder. All rights reserved. No reuse allowed without permission.

Titan cells are structurally distinct from those produced by typical yeast cells (7, 11, 26). As the increased chitin content of cell walls produced by Titan cells is associated with activation of a detrimental T_H2 immune response during cryptococcosis (27), it is possible that hitherto unidentified structural differences in Titan cell capsules also contribute to the modulation of host immunity by this *C. neoformans* morphotype.

Alterations in capsule structure are likely to affect how *Cryptococcus* is perceived by host immune molecules, with antibodies particularly sensitive to small changes in molecular structures. Following exposure to cryptococci, immunoglobulin M (IgM) antibodies are the most abundant isotype of antibody produced in response to GXM (28). As a repetitive capsular polysaccharide, GXM is a T-independent type 2 antigen and antibodies generated against it utilise a restricted set of variable region gene segments (29). Using monoclonal antibodies (mAbs) in conjunction with mutants harbouring specific defects in GXM modification (17, 30, 31), it has been determined that *O*-acetylation and, to a lesser extent, xylosylation of GXM are important for epitope recognition by anti-GXM antibodies (16, 30). Whilst there is no consensus surrounding the effect of GXM *O*-acetylation on virulence (17, 32), its influence on antibody binding suggests that changes in GXM *O*-acetylation could be a strategy deployed by cryptococci to avoid recognition by immune effectors. Additionally, despite the immunomodulatory roles for GXM *O*-acetylation that have been identified (30, 33), receptors that bind *O*-acetylated GXM remain elusive (34). Due to the enigmatic nature of this modification within the primary virulence factor of cryptococci, further investigation of GXM *O*-acetylation will help unravel the

bioRxiv preprint doi: https://doi.org/10.1101/431650; this version posted October 1, 2018. The copyright holder for this preprint (which was not certified by peer review) is the author/funder. All rights reserved. No reuse allowed without permission.

143 complexities of cryptococcal capsule structure with the ultimate aim of understanding
144 the strategies deployed by this fatal fungal pathogen to evade host immunity.
145
146 In the present study, we report the generation of Crp127, a murine IgM mAb, using a
147 cocktail of heat-killed *C. neoformans* H99 (serotype A), heat-killed *C. gattii* R265
148 (serotype B) and their lysates as an immunogen. Characterisation of Crp127
149 demonstrated that it is an *O*-acetyl-dependent anti-GXM mAb specific to an epitope
150 expressed by the four *Cryptococcus* serotypes in a serotype-specific manner. Having
151 subsequently found that this epitope is heterogeneously expressed within serotype B
152 populations and is spatially confined to distinct regions of the enlarged capsule
153 across all strains tested, we then turned our attention to its expression by Titan cells.
154 Intriguingly, we noticed that the spatial distribution of this epitope differs within the
155 capsules produced by the three *C. neoformans* morphotypes found within Titanising
156 populations. Further analysis revealed that, under conditions permissive for
157 Titanisation, cell enlargement coincides with the gradual redistribution of this epitope
158 to the capsule surface.
159
160 **Results**
161 **Crp127 recognises a capsular epitope located in GXM**
162 During hybridoma screening, Crp127 was identified as staining the outer zone of live
163 cryptococci. We first assessed whether Crp127 recognises a capsular component by
164 performing flow cytometric analysis of three GXM-deficient mutants (R265 *cap10*Δ*,*
165 Kn99α *cap59*Δ and B3501 *cap67*Δ*)*, a GXMGal-deficient mutant (Kn99α *uge1*Δ) and
166 a mutant lacking both GXM and GXMGal (Kn99α *cap59*Δ*uge1*Δ), using an Alexa-
167 488-conjugated anti-IgM secondary antibody to label Crp127. Unlike their

bioRxiv preprint doi: https://doi.org/10.1101/431650; this version posted October 1, 2018. The copyright holder for this preprint (which was not certified by peer review) is the author/funder. All rights reserved. No reuse allowed without permission.

corresponding wild-type strains, the GXM-deficient mutants were not recognised by Crp127 (fig. 1A-C; *cap10*Δ $P < 0.05$; *cap67*Δ $P < 0.01$; *cap59*Δ $P < 0.01$; *cap59*Δ*uge1*Δ $P < 0.01$, Student's t-test). In contrast, the GXMGal-deficient *uge1*Δ mutant was bound at levels similar to the wild-type strain (fig. 1C; $P > 0.05$). Confocal microscopy corroborated these observations, with no observable binding of Crp127 to GXM-deficient mutants but clear binding of Crp127 to the GXMGal-deficient mutant (fig. 1D-F). Taken together, these experiments demonstrated that the epitope recognised by Crp127 – hereon referred to as the Crp127 epitope – is a component of GXM.

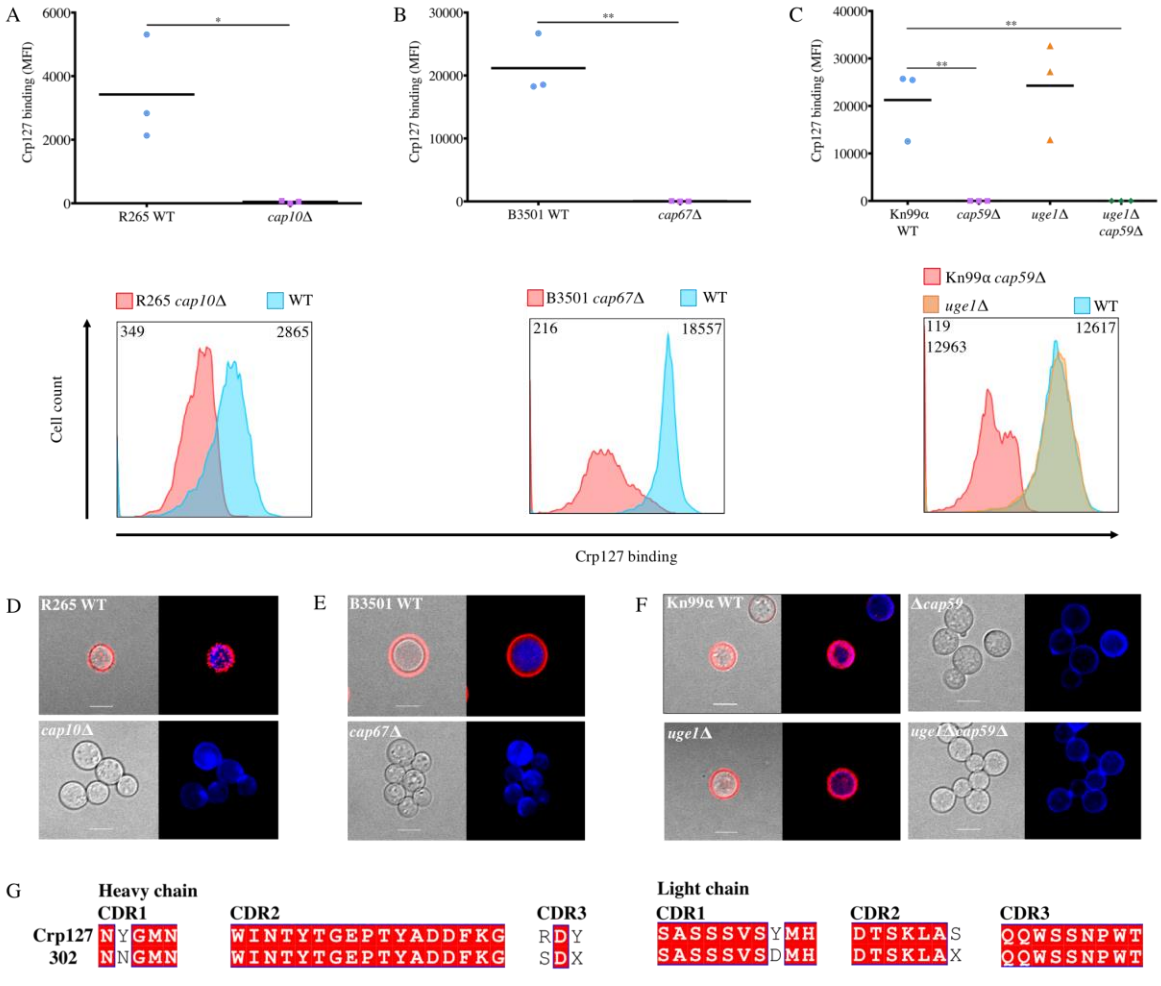

Fig. 1. Crp127 is an anti-GXM mAb. *The ability of Crp127 to bind to GXM- and GXMGal-deficient mutants of C. gattii and C. neoformans was quantified via flow*

bioRxiv preprint doi: https://doi.org/10.1101/431650; this version posted October 1, 2018. The copyright holder for this preprint (which was not certified by peer review) is the author/funder. All rights reserved. No reuse allowed without permission.

cytometry. Scatter plots (top row) and representative histograms (bottom row) are presented for ***A)*** *R265 cap10Δ,* ***B)*** *B3501 cap67Δ,* ***C)*** *Kn99α cap59Δ, Kn99α uge1Δ, Kn99α cap59Δuge1Δ and their corresponding wild-type strains. For scatter plots, corrected median fluorescence intensity (MFI) values were calculated by subtracting the MFI value of isotype control cells from the MFI value of the Crp127-treated cells, with data points representing MFI values calculated from three biological replicates performed as independent experiments. A Student's t-test was used to test for statistically significant differences between R265 cap10Δ and B3501 cap67Δ and their corresponding wild-type strains, whilst one-way ANOVA followed by Dunnett's multiple comparison test was used to test for statistically significant differences between Kn99α cap59Δ, Kn99α uge1Δcap59Δ, Kn99α uge1Δ and the wild-type strain KN99α (n=3) (ns P > 0.05; * P < 0.05; ** P < 0.01). Histograms show a representative distribution of Crp127 binding for one or all of the strains in the above scatter plot, with the colour-coded key provided for reference. Numerical values in the top left and right of each histogram correspond to the MFI value calculated from the strain labelled directly above.* ***D)*** *R265 cap10Δ,* ***E)*** *B3501 cap67Δ,* ***F)*** *Kn99α cap59Δ, uge1Δ, uge1Δcap59Δ and their wild-type strains were labelled for chitin using calcofluor-white (CFW; blue) and Crp127 (far-red; goat Alexa-647-conjugated anti-mouse IgM μ-chain) and maximum-intensity projections generated from confocal microscopy z-stacks. Presented are representative images merged for transmitted light and Crp127 (left panels) and Crp127 and chitin (right panels). Scale bars represent 5 μm.* ***G)*** *Amino acid sequences of the CDRs from mAbs Crp127 and 302 were aligned. Residues highlighted in red are identical. X denotes amino acid residues that are undetermined.*

bioRxiv preprint doi: https://doi.org/10.1101/431650; this version posted October 1, 2018. The copyright holder for this preprint (which was not certified by peer review) is the author/funder. All rights reserved. No reuse allowed without permission.

In order to draw comparisons with previously described anti-GXM mAbs, we next sequenced both the heavy-chain variable (V_H) and light-chain variable (V_L) regions of Crp127 (fig. S1). Antibody sequence analysis revealed that the Crp127 V_H region uses the V_H9(VGAM family)-J_H2 combination with a D-segment consisting of four amino acids, whilst the V_L region uses a combination of V_k4/5-J_k1. This gene usage profile is remarkably similar to that of anti-GXM IgG1 mAb 302, which differs only in respect to the length of its D-segment (35). In line with this, alignment of Crp127 and 302 protein sequences revealed 86.6% and 98.1% sequence identity between V_H and V_L regions, respectively (fig. S1A-B). When the complementarity determining regions (CDRs) of mAbs Crp127 and 302 were aligned, we found identical V_H CDR2 and V_L CDR3 regions whilst the remaining CDRs differed at one or two positions (fig. 1G). Notably, however, the sequence available for mAb 302 is incomplete and may contribute additional variation (fig. 1G). We also compared the CDRs of Crp127 with four other well-characterised anti-GXM IgM mAbs – 2D10, 12A1, 13F1 and 21D2 – with less similarities identified between Crp127 and these mAbs (fig. S1C-D).

GXM *O*-acetylation is required for Crp127 epitope recognition

Considering the importance of *O*-acetylation and xylosylation to the antigenic signature of GXM (30), we proceeded to investigate the effect of these modifications on Crp127 epitope recognition. We firstly tested the ability of Crp127 to recognise two xylose-deficient mutants (JEC155 *uxs1*Δ (serotype D) and Kn99α *uxs1*Δ (serotype A)). No significant differences were found between either *uxs1*Δ mutant and their corresponding wild-type strains (fig. 2A; JEC155 *uxs1*Δ $P > 0.05$; Kn99α *uxs1*Δ $P > 0.05$), indicating that xylosylation does not impact Crp127 binding. In contrast, however, antibody binding was completely abrogated in the *O*-acetyl-

bioRxiv preprint doi: https://doi.org/10.1101/431650; this version posted October 1, 2018. The copyright holder for this preprint (which was not certified by peer review) is the author/funder. All rights reserved. No reuse allowed without permission.

deficient *cas1*Δ mutant (fig. 2B; $P < 0.01$), indicating that *O*-acetylation of GXM is an essential prerequisite for Crp127 epitope recognition.

Having made this observation, we proceeded to test two further mutants in genes implicated in GXM *O*-acetylation. Kn99α *cas3*Δ exhibits a ~70% reduction in GXM *O*-acetylation, whereas Kn99α *cas31*Δ exhibits subtle differences in sugar composition of GXM but no reduction in GXM *O*-acetylation (36). Binding of Crp127 to the *cas3*Δ mutant was slightly reduced but statistically to the wild-type strain (fig. 2C; $P > 0.05$). This may reflect reduced density of *O*-acetylation in GXM produced by this mutant Surprisingly, however, Crp127 completely failed to recognise the *cas31*Δ mutant despite this strain retaining an *O*-acetylation profile similar to the wild-type (36) (fig. 2C; $P < 0.01$). To be certain that the *O*-acetyl-defective mutants tested still produced capsule, we confirmed the binding of *O*-acetyl-independent anti-GXM mAb F12D2 to each strain (fig. 2E-F; insets). Thus, *CAS1* and *CAS31* contribute to the formation of an *O*-acetylation dependent Crp127 epitope.

bioRxiv preprint doi: https://doi.org/10.1101/431650; this version posted October 1, 2018. The copyright holder for this preprint (which was not certified by peer review) is the author/funder. All rights reserved. No reuse allowed without permission.

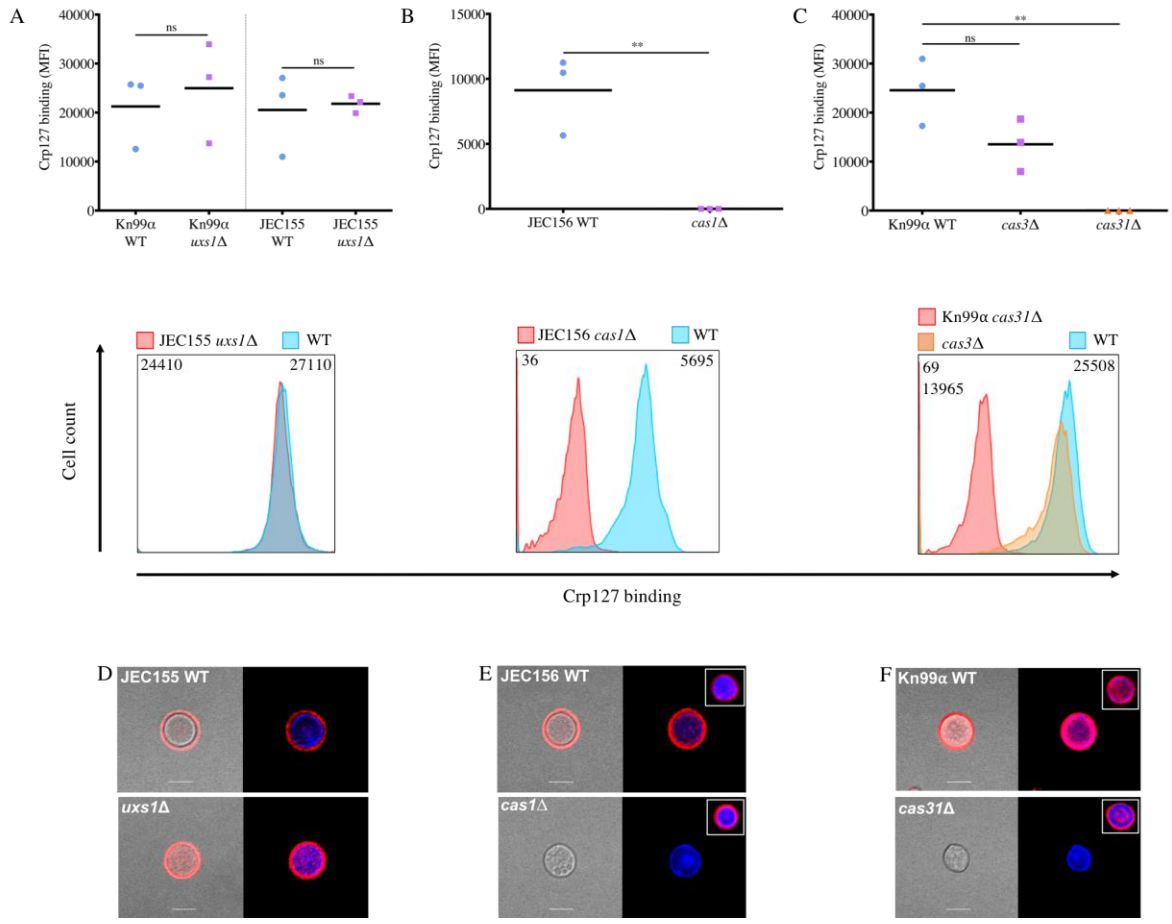

246

247 ***Fig. 2. Crp127 requires O-acetylation, but not xylosylation, of GXM for epitope***
248 ***recognition.*** *The ability of Crp127 to recognise mutants with specific defects in GXM*
249 *modification was quantified via flow cytometry. Scatter plots (top row) and*
250 *representative histograms (bottom row) are presented for* ***A)*** *Kn99α uxs1Δ, JEC155*
251 *uxs1Δ and corresponding wild-type strains;* ***B)*** *JEC156 cas1Δ and JEC155 wild-type*
252 *and* ***C)*** *Kn99α cas3Δ, Kn99α cas31Δ and Kn99α wild-type. For scatter plots,*
253 *corrected MFI values were calculated by subtracting the MFI value of isotype control*
254 *cells from the MFI value of the Crp127-treated cells, with data points representing*
255 *MFI values calculated from three biological replicates performed as independent*
256 *experiments. A Student's t-test was used to test for statistically significant differences*
257 *between Kn99α uxs1Δ, JEC155 uxs1Δ and JEC156 cas1Δ and their corresponding*
258 *wild-type strain whilst Dunnet's multiple comparison test was used to test for*

bioRxiv preprint doi: https://doi.org/10.1101/431650; this version posted October 1, 2018. The copyright holder for this preprint (which was not certified by peer review) is the author/funder. All rights reserved. No reuse allowed without permission.

*statistically significant differences between Kn99α Δcas3, Kn99α Δcas31 mutants and the Kn99α wild-type strain (n=3) (ns P > 0.05; * P < 0.05; ** P < 0.01). Histograms show a representative distribution of Crp127 binding for one or all of the strains in the above scatter plot, with a colour-coded key provided for reference. Numerical values in the top left and right of each histogram correspond to the MFI value calculated from the strain labelled directly above.* ***D)*** *JEC155 uxs1Δ,* ***E)*** *JEC156 cas1Δ,* ***F)*** *Kn99α cas31Δ and corresponding wild-type strains were labelled for chitin (blue; CFW) and Crp127 (far-red; goat Alexa-647-conjugated goat anti-mouse IgM μ-chain) and maximum-intensity projections generated via confocal microscopy. Presented are representative images merged for transmitted light and Crp127 (left panels) and Crp127 and chitin (right panels). Insets in the top right of images show representative cells labelled for chitin (blue) and O-acetyl-independent mAb F12D2 (far-red; Alexa-647-conjugated F(ab')2 goat anti-Mouse IgG (H+L)) used as a control. Scale bars represent 5 μm.*

Lastly, we confirmed that GXM *O*-acetylation is essential for Crp127 recognition by testing the binding of Crp127 to *Cryptococcus* cells that had been chemically de-*O*-acetylated via alkaline hydrolysis. For both strains tested (H99 and B3501), Crp127 failed to bind chemically de-*O*-acetylated cells, just as it failed to recognise the *cas1Δ* mutant (fig. S2A-C; H99 $P < 0.01$ and B3501 $P < 0.01$). However, binding of *O*-acetylation independent antibodies F12D2 and 18B7 remained unaltered (fig. S2C-D; $P > 0.05$). Taken together, our results demonstrate an essential role for *O*-acetylation in recognition of GXM by Crp127.

Cryptococcus serotypes differ in their level of Crp127 epitope recognition

bioRxiv preprint doi: https://doi.org/10.1101/431650; this version posted October 1, 2018. The copyright holder for this preprint (which was not certified by peer review) is the author/funder. All rights reserved. No reuse allowed without permission.

284 Differences in the *O*-acetylation state of GXM contributes towards serotype
285 classification and is a source of structural variation within the capsule of cells from a
286 clonal population (21, 30). Therefore, with Crp127 recognising an *O*-acetyl-
287 dependent epitope, we next checked for differences in Crp127 staining between the
288 five recognised serotypes of *Cryptococcus neoformans* and *gattii*, testing two
289 independent strains of each serotype. Flow cytometry analysis demonstrated that
290 Crp127 consistently bound most effectively to serotype D strains (B3501 and
291 JEC155) (fig. 3A-B), with all cells within these populations exhibiting high-level
292 accessibility of the Crp127 epitope (fig. 3F). We detected slightly lower binding to
293 serotype A strains (fig. 3A-B), with high-level homogeneous staining also seen in the
294 case of H99, but a proportion of unstained cells from strain Kn99α (fig. 3C).
295 Interesting, the two AD hybrid strains tested (CBS 950 and ZG287) were notably
296 different in regard to Crp127 binding (fig. 3A-B), with CBS 950 exhibiting low-level
297 heterogeneous staining and ZG287 showing high-level homogeneous staining (fig.
298 3G).
299
300 The two remaining cryptococcal serotypes, B and C, together represent *C. gattii*.
301 Serotype B strains R265 and CDCR272 demonstrated significantly lower epitope
302 recognition than *C. neoformans* serotypes (fig. 3A-B) and considerable heterogeneity
303 within the population (fig. 3D). Interestingly, however, serotype C strains were
304 completely unrecognised by Crp127, with neither strain CBS 10101 or M27055
305 showing detectable staining (fig. 3A, B and E). From this, we conclude that there are
306 serotype-specific differences in the availability of the Crp127 epitope, with epitope
307 accessibility being related to serotype in a pattern of D > A >> B >>> C.
308

bioRxiv preprint doi: https://doi.org/10.1101/431650; this version posted October 1, 2018. The copyright holder for this preprint (which was not certified by peer review) is the author/funder. All rights reserved. No reuse allowed without permission.

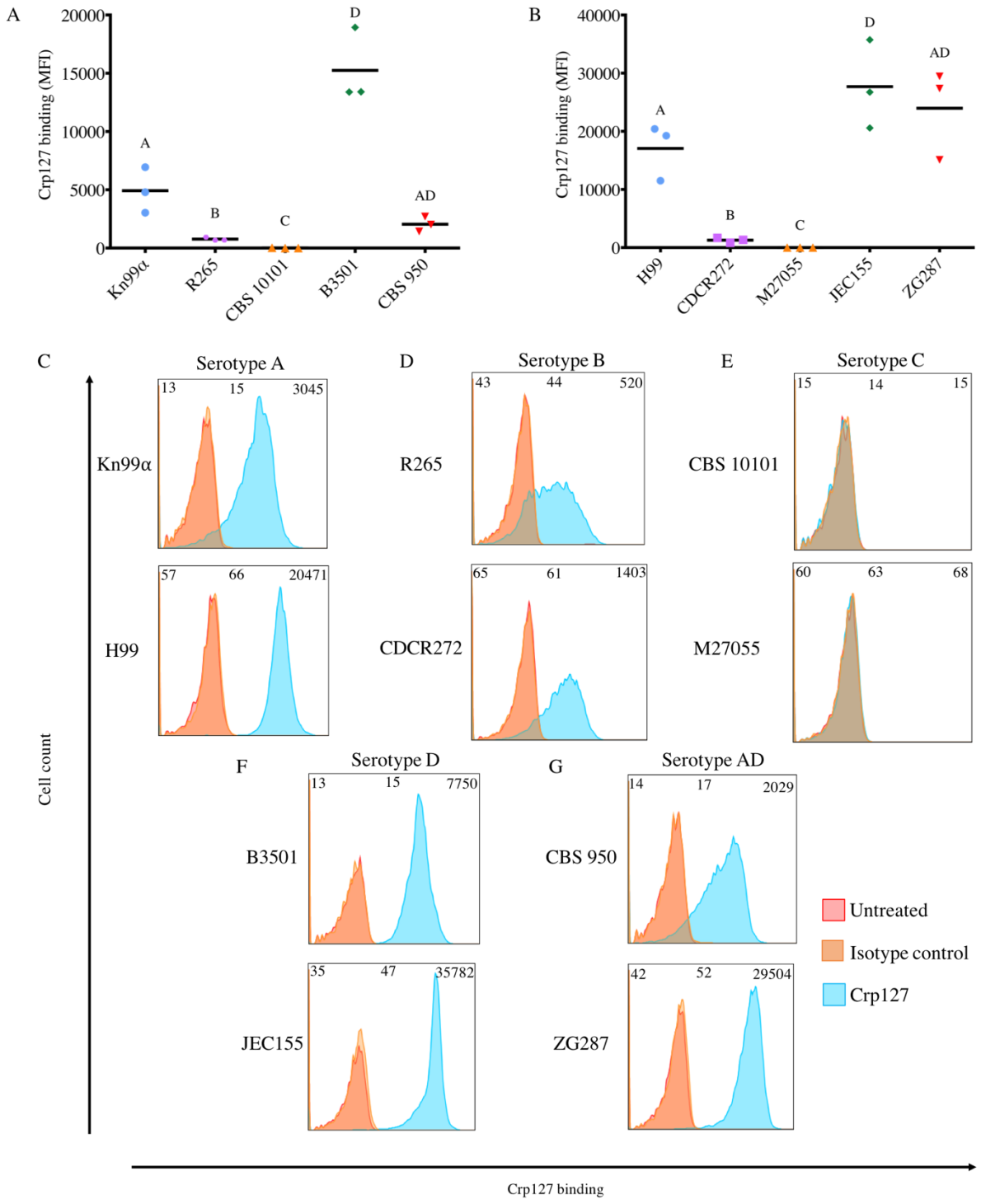

Fig. 3. Recognition levels of the Crp127 epitope are associated with serotype. *The ability of Crp127 to bind to two different strains from each Cryptococcus serotypes A, B, C, D and AD was quantified using flow cytometry.* ***A-B)*** *Scatter plots show corrected MFI values for each strain, which were calculated by subtracting the MFI value of isotype control cells from the MFI value of the corresponding Crp127-*

bioRxiv preprint doi: https://doi.org/10.1101/431650; this version posted October 1, 2018. The copyright holder for this preprint (which was not certified by peer review) is the author/funder. All rights reserved. No reuse allowed without permission.

treated cells. Data points represent MFI values calculated from three biological replicates performed as independent experiments (n=3). Histograms show a representative distribution of Crp127 binding for ***C)*** *serotype A strains Kn99α and H99,* ***D)*** *serotype B strains R265 and CDCR272,* ***E)*** *serotype C strains CBS 10101 and M27055,* ***F)*** *serotype D strains B3501 and JEC155 and* ***G)*** *serotype AD hybrid strains CBS 950 and ZG287. Fluorescence intensity values for untreated, isotype control and Crp127-treated cells are presented in red, blue and orange, respectively, with corresponding MFI values displayed in the top left, centre and right of each panel.*

Crp127 exhibits serotype-specific binding patterns that are not associated with opsonic efficacy

Having identified differential levels of the Crp127 epitope between serotypes using flow cytometry, we next examined their patterns of binding by immunofluorescence microscopy. Indirect immunofluorescence revealed an annular binding pattern for all four strains representing serotypes A and D (fig. 4A and D). In line with their differences in flow cytometry, the two AD hybrid strains tested showed different patterns of binding, with CBS 950 showing punctate binding and ZG287 showing a mix of annular and punctate staining. Both *C. gattii* serotype B strains exhibited punctate binding (fig. 4B and E) whilst, in agreement with flow cytometry, no Crp127 binding was detected when imaging serotype C strains CBS 10101 or M27055. However, *O*-acetyl-independent mAb F12D2 bound well to these strains, suggesting that the lack of Crp127 binding reflects changes in GXM *O*-acetylation rather than loss of capsular material (fig. 4C; inset).

bioRxiv preprint doi: https://doi.org/10.1101/431650; this version posted October 1, 2018. The copyright holder for this preprint (which was not certified by peer review) is the author/funder. All rights reserved. No reuse allowed without permission.

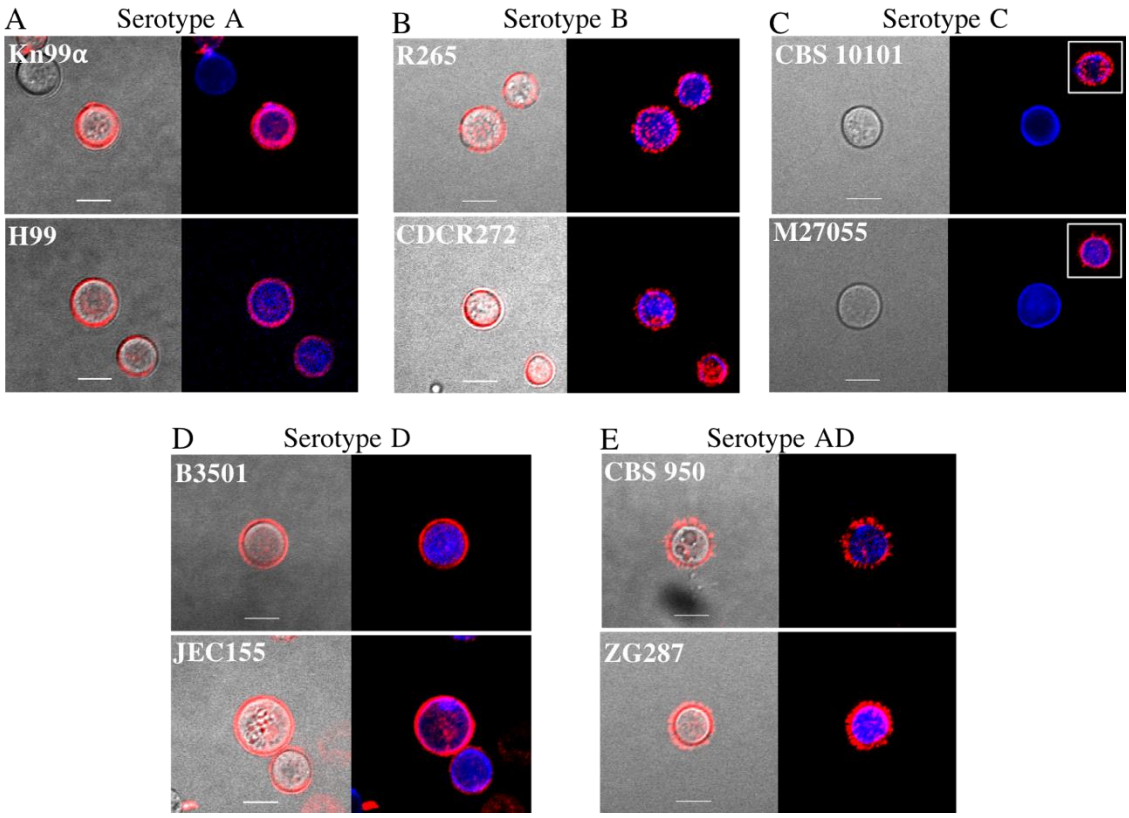

Fig. 4. The immunofluorescence-binding pattern of Crp127 correlates with serotype. *Two Cryptococcus strains from* ***A)*** *serotype A (Kn99 and H99),* ***B)*** *serotype B (R265 and CDCR272),* ***C)*** *serotype C (CBS 10101 and M27055),* ***D)*** *serotype D (B3501 and JEC155) and* ***E)*** *serotype AD (CBS 950 and ZG287) were labelled for chitin (blue; CFW) and Crp127 (far-red; goat Alexa-647-conjugated anti-mouse IgM μ-chain) and maximum-intensity projections generated via confocal microscopy. Representative images are shown for each strain. Images are merged for transmitted light and Crp127 (left panels) and Crp127 and chitin (right panels). Insets in the top right of images show representative cells labelled for chitin (blue) and O-acetyl-independent mAb F12D2 (far-red; Alexa-647-conjugated F(ab')2 goat anti-Mouse IgG (H+L)). Scale bars represent 5 μm.*

bioRxiv preprint doi: https://doi.org/10.1101/431650; this version posted October 1, 2018. The copyright holder for this preprint (which was not certified by peer review) is the author/funder. All rights reserved. No reuse allowed without permission.

354 As annular and punctate binding patterns have been associated with opsonic and
355 non-opsonic anti-GXM IgM mAbs, respectively, we tested the ability of Crp127 to
356 opsonise cells from strains Kn99α (annular) and R265 (punctate). Unlike positive
357 control treatments mAb 18B7 and pooled human serum, Crp127 did not enhance
358 phagocytosis of either strain by J774 macrophage-like cells in the presence or
359 absence of serum (fig. S3). In summary, annular binding patterns are associated
360 with the high-level binding of Crp127 to *C. neoformans* serotypes A and D strains.
361 On the other hand, punctate binding is associated with low-level binding of Crp127 to
362 serotype B strains. However, under the conditions tested in this study, neither
363 binding pattern is clearly associated with opsonic efficacy.
364
365 **Crp127 epitope recognition reflects serotype differences within *C. gattii***
366 Our data above indicate that Crp127 binding accurately reflects known serotyping of
367 cryptococcal strains. However, recent genomic data indicate that *C. gattii* may in fact
368 be composed of several cryptic species (37). We therefore extended our analysis of
369 this species group by investigating a further four *C. gattii* strains, representing
370 molecular subtypes VGI-VGIII. Similar levels of Crp127 epitope recognition was seen
371 for serotype B strains R265 (VGIIa), CDCR272 (VGIIb), EJB55 (VGIIc) and CA1873
372 (VGIIIa) (fig. 5A-B; $P > 0.05$), however significantly higher recognition was seen for
373 the serotype B strain DSX (VGI) (fig. 5A-B; $P < 0.01$). Indirect immunofluorescence
374 corroborated these findings, with punctate binding seen for the four strains
375 presenting the epitope at low levels (fig. 5D-H) and annular binding seen for strain
376 DSX (fig. 5C). We also tested strain CA1508 (VGIIIb), a *C. gattii* strain that, to our
377 knowledge, has not previously been serotyped. Both flow cytometry and indirect
378 immunofluorescence showed that Crp127 did not recognise this strain (fig. 5A and

bioRxiv preprint doi: https://doi.org/10.1101/431650; this version posted October 1, 2018. The copyright holder for this preprint (which was not certified by peer review) is the author/funder. All rights reserved. No reuse allowed without permission.

H), implying that it is a serotype C strain. In combination with the data presented in figure 3, our finding that four out of five serotype B strains were bound similarly by Crp127 suggests that availability of this epitope is fairly well conserved within this serotype.

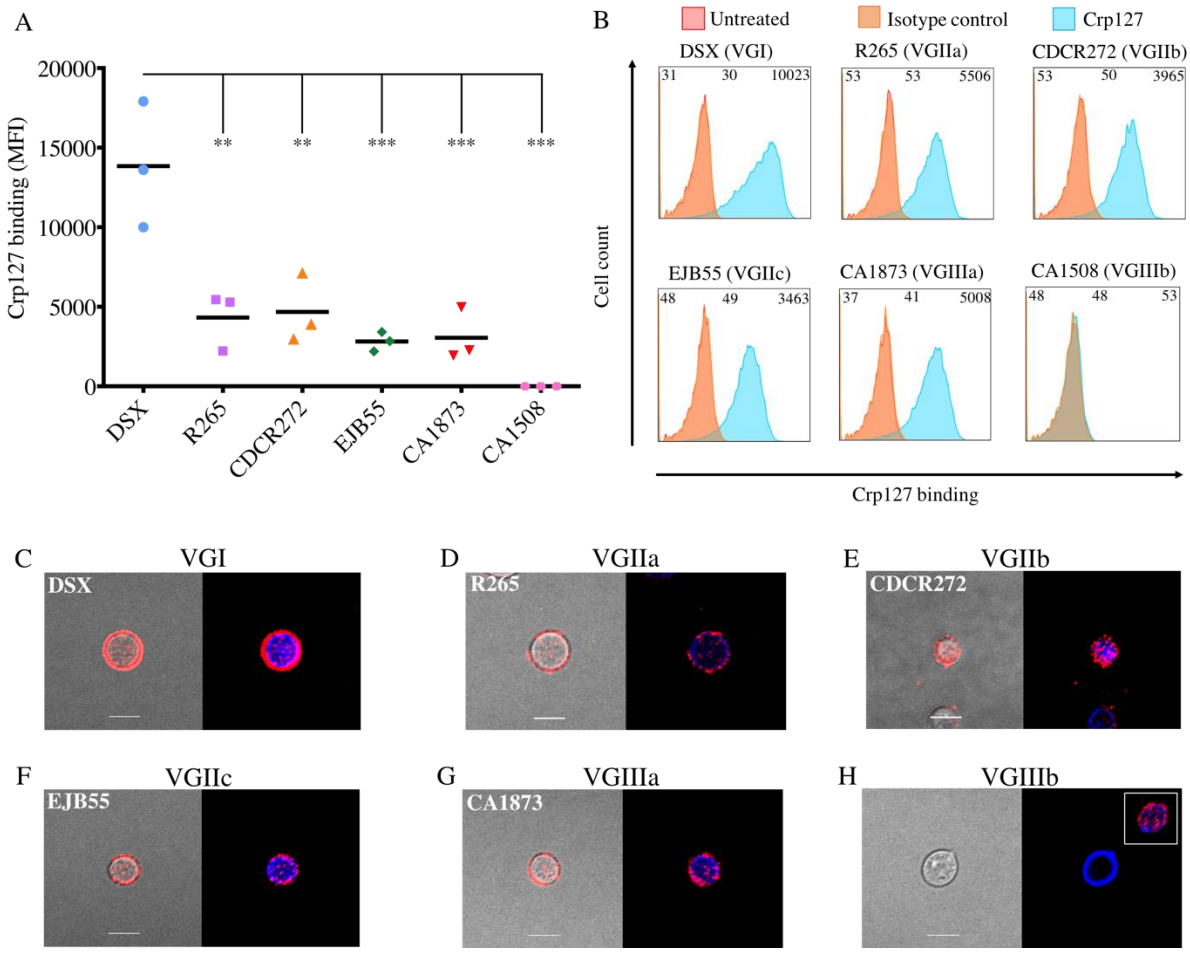

Fig. 5. Recognition of the Crp127 epitope is largely consistent within C. gattii serotypes. *The ability of Crp127 to bind to six strains from C. gattii that encompass molecular types VGI-VGIIIb was quantified via flow cytometry.* ***A)*** *Scatter plots show corrected MFI values for each strain, which were calculated by subtracting the MFI value of isotype control cells from the MFI value of the corresponding Crp127-treated cells. Data points represent MFI values calculated from three biological replicates performed as independent experiments. Tukey's multiple comparisons test was used to test the statistical significance of differences between the six strains (n=3) (ns P >*

bioRxiv preprint doi: https://doi.org/10.1101/431650; this version posted October 1, 2018. The copyright holder for this preprint (which was not certified by peer review) is the author/funder. All rights reserved. No reuse allowed without permission.

*0.05; ** P < 0.01; *** P < 0.001).* ***B)*** *Histograms show a representative distribution of Crp127 binding for strains DSX (VGI), R265 (VGIIa), CDCR272 (VGIIb), EJB55 (VGIIc), CA1873 (VGIIIa) and CA1508 (VGIIIb). Fluorescence intensity values for untreated, isotype control and Crp127-treated cells are presented in red, blue and orange, respectively, with corresponding MFI values displayed in the top left, centre and right of each panel. C. gattii strains* ***C)*** *DSX,* ***E)*** *R265,* ***F)*** *CDCR272,* ***G)*** *CA1873 and* ***H)*** *CA1508 were labelled for chitin (blue; CFW) and Crp127 (far-red; goat Alexa-647-conjugated anti-mouse IgM μ-chain) and maximum-intensity projections generated via confocal microscopy. Presented are representative images merged for transmitted light and Crp127 (left panels) and Crp127 and chitin (right panels). Scale bars represent 5 μm. Insets in the top right of images show representative cells labelled for chitin (blue) and O-acetyl-independent mAb F12D2 (far-red; Alexa-647-conjugated F(ab')2 goat anti-Mouse IgG (H+L)). Scale bars represent 5 μm.*

The Crp127 epitope localises to spatially confined zones of the enlarged capsule and binding elicits capsular swelling reactions

Having investigated the binding of Crp127 to cells with a small capsule, we next wished to investigate cells that had been grown in capsule-inducing conditions, given that capsule enlargement occurs shortly after infection of the host. Interestingly, in all of the strains tested we saw that the Crp127 epitope was spatially confined to distinct capsular regions (fig. 6). For serotype A and D strains, antibody binding was detected in the central zone of the capsule (fig. 6A and D). Serotype B strains differed, with regions adjacent to the cell wall and on the capsule surface bound by Crp127 in the case of strain R265 but only the single region proximal to the surface bound in the case of CDCR272 (fig. 6B). Serotype AD strain ZG287 exhibited a

bioRxiv preprint doi: https://doi.org/10.1101/431650; this version posted October 1, 2018. The copyright holder for this preprint (which was not certified by peer review) is the author/funder. All rights reserved. No reuse allowed without permission.

similar pattern of binding to R265, with Crp127 binding to both an inner and outer region of the capsule, however strain CBS 950 was bound in a region adjacent to the cell wall (fig. 6D).

The binding of mAbs to capsular GXM alters the refractive index of the enlarged capsule, resulting in capsular swelling reactions that can be visualised using DIC microscopy (38). In testing the ability of Crp127 to produce a capsular swelling reaction with strains Kn99α, R265, B3501 and CBS 950, we observed no discernible differences in the reaction pattern produced between strains, with a highly refractive outer rim and a textured inner capsule characteristic for each strain (fig. 6E-H; left panels). Notably, however, Crp127 reaction patterns differed from those elicited by 18B7, which also exhibited a highly refractive outer rim but lacked texture throughout the capsule (fig. 6E-H; right panels). Taken together, our studies of Crp127 binding to capsule-induced cells demonstrate that the Crp127 epitope is localised to specific capsular regions and that Crp127 binding produces capsular swelling reactions that are independent of serotype.

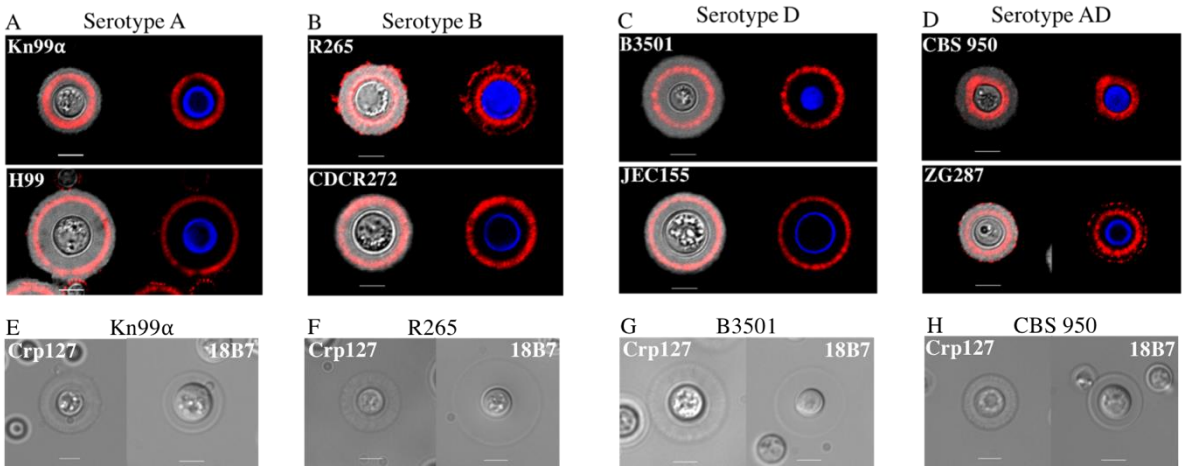

Fig. 6. The Crp127 epitope is spatially confined to distinct capsular regions and binding elicits capsular swelling reactions distinct from those of 18B7.

bioRxiv preprint doi: https://doi.org/10.1101/431650; this version posted October 1, 2018. The copyright holder for this preprint (which was not certified by peer review) is the author/funder. All rights reserved. No reuse allowed without permission.

436 *Cryptococcus cells were grown in capsule-inducing conditions and imaged to*
437 *determine the location of the Crp127 epitope within the enlarged capsule and*
438 *characterise the capsular reaction patterns elicited by this antibody. Cryptococcus*
439 *strains from **A)** serotype A (Kn99α and H99), **B)** serotype B (R265 and CDCR272,*
440 ***C)** serotype D (B3501 and JEC155) and **D)** serotype AD (CBS 950 and ZG287) were*
441 *labelled for chitin (blue; CFW) and Crp127 (far-red; goat Alexa-647-conjugated anti-*
442 *mouse IgM μ-chain), suspended in Indian ink to visualise the capsule and imaged*
443 *using confocal microscopy. Representative images of a single focal plane are shown*
444 *for each strain. Presented are images merged for transmitted light and Crp127 (left*
445 *panels) and Crp127 and chitin (right panels). Capsule-induced cells of strains **E)***
446 *Kn99α, **F)** R265, **G)** B3501 and **H)** CBS 950 were also treated with either Crp127*
447 *(left panels) or 18B7 (right panels) and imaged using DIC microscopy to observe*
448 *capsular reaction patterns. Scale bars represent 5 μm.*
449
450 **Spatial distribution of the Crp127 epitope differs within the capsules produced**
451 **by Titanide, yeast-like and Titan cells**
452 Following infection of the host lung, a proportion of *C. neoformans* cells differentiate
453 into Titan cells, a very large morphotype that facilitates pathogenesis and is
454 associated with poor clinical outcomes (8, 12). When grown under Titanising
455 conditions *in vitro*, *C. neoformans* forms a heterogeneous population of small oval-
456 shaped Titanide cells (<5 μm cell body diameter), yeast-like cells (~5 μm) and large
457 Titan cells (>10 μm) (9). As differences in capsule structure – but not mAb binding
458 pattern – are known to exist between yeast and Titan cells (26, 39), we tested
459 whether Crp127 could distinguish the morphological subtypes found in Titanising
460 populations from strains H99 and Kn99α. Indeed, when imaging cells grown in

bioRxiv preprint doi: https://doi.org/10.1101/431650; this version posted October 1, 2018. The copyright holder for this preprint (which was not certified by peer review) is the author/funder. All rights reserved. No reuse allowed without permission.

Titanising conditions *in vitro*, we noticed differences in the spatial distribution of the Crp127 epitope within the capsules produced by cells of different sizes (fig. 7A). Specifically, Crp127 bound to a capsular region adjacent to the cell wall in smaller Titanide cells, within the central zone of the capsule in yeast-like cells and close to the capsule surface of Titan cells. In order to quantify how cell size affects capsular distribution of the Crp127 epitope, we determined the ratio between the area of capsule encompassed by the Crp127 epitope and the area of the whole capsule; using this metric, a ratio approaching 1 is indicative of the epitope being found in close proximity to the capsule surface (fig. 7B). Across three biological repeats (with a mean number of 111 and 133 cells measured for strains H99 and Kn99α, respectively), mean (± standard error of the mean) ratios of 0.28 ± 0.04 and 0.30 ± 0.03 were calculated for Titanide cells (<5 μm in diameter) for strains H99 and Kn99α, respectively, consistent with our initial observations that the Crp127 bound near to the cell wall of these small cells (fig. 7C-D). For yeast-like cells (5-10 μm in diameter), mean ratios were 0.42 ± 0.03 and 0.39 ± 0.02 for strains H99 and Kn99α, respectively (fig. 7C-D), indicating the Crp127 epitope is predominantly located in the central zone of the capsule in yeast-like cells, as we had previously observed (fig. 6A). Finally, the mean ratios for Titan cells (>10 μm in diameter) were 0.72 ± 0.03 and 0.71 ± 0.03 for strains H99 and Kn99α respectively, making them significantly higher than those calculated for both Titanide (fig. 7C-D; H99 $P < 0.001$; Kn99α $P < 0.001$) and yeast-like cells (fig. 7C-D; H99 $P < 0.01$; Kn99α $P < 0.001$). In summary, our results demonstrate that Crp127 binds closer to the capsule surface of Titan cells than Titanide and yeast-like cells.

bioRxiv preprint doi: https://doi.org/10.1101/431650; this version posted October 1, 2018. The copyright holder for this preprint (which was not certified by peer review) is the author/funder. All rights reserved. No reuse allowed without permission.

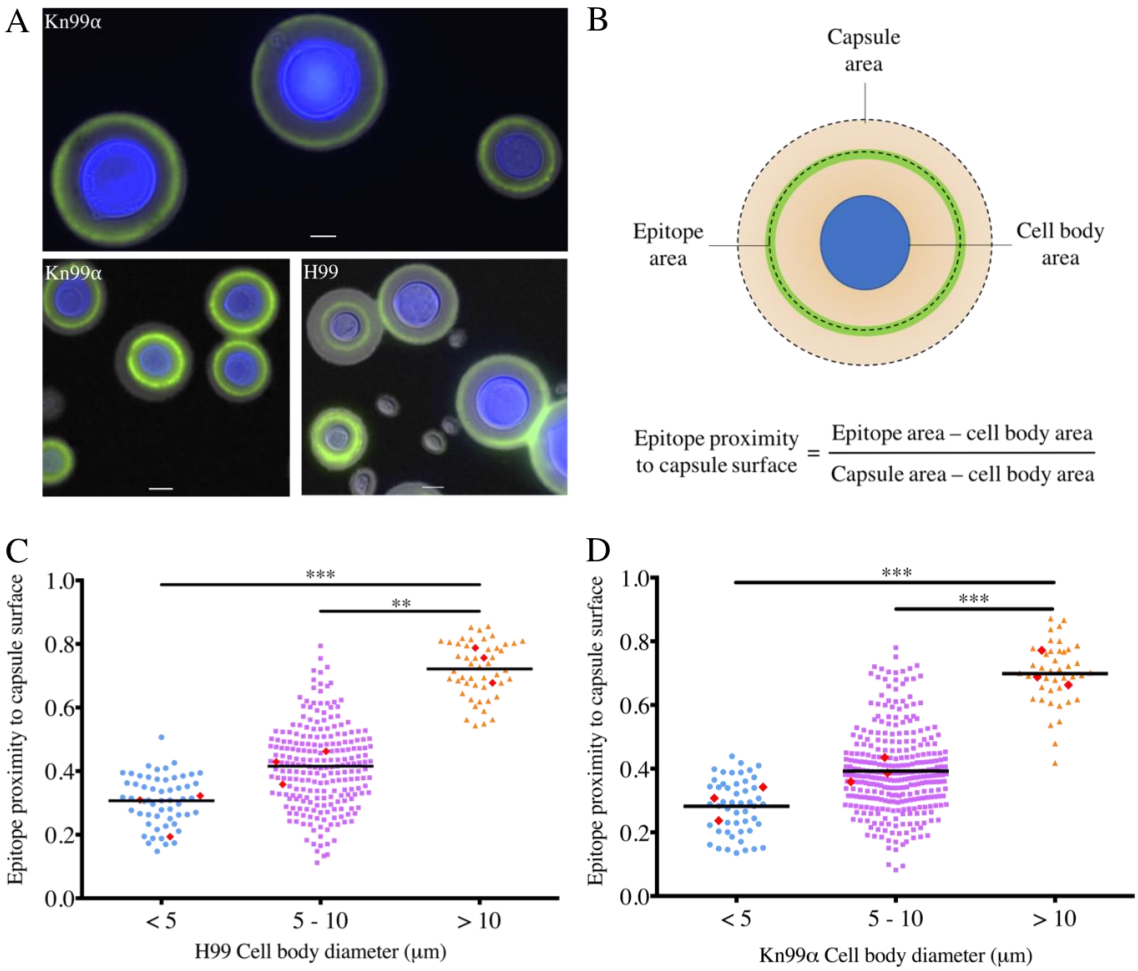

Fig. 7. Spatial distribution of the Crp127 epitope differs within the capsule of the three cell subtypes found in Titanising populations. *Cultures of C. neoformans strains H99 and Kn99α that derived solely from Titan cells were investigated for differences in the capsular distribution of the Crp127 epitope.* ***A)*** *Representative images of cells from strains H99 and Kn99α grown under conditions permissive for Titanisation. Scale bars represent 5 μm.* ***B)*** *A schematic representation of how Crp127 epitope proximity to the capsule surface was quantified through the analysis of micrographs using ImageJ software. The proximity of the Crp127 epitope to the capsule surface of* ***C)*** *H99 and* ***D)*** *Kn99α cells with cell body diameter <5 μm (blue circles), 5-10 μm (purple squares) and >10 μm (orange triangles) was quantified. Data points represent all individual cells for which the*

bioRxiv preprint doi: https://doi.org/10.1101/431650; this version posted October 1, 2018. The copyright holder for this preprint (which was not certified by peer review) is the author/funder. All rights reserved. No reuse allowed without permission.

*location of the Crp127 epitope was quantified, whilst the horizontal bar represents the mean. Red diamonds represent mean values calculated from three biological repeats. Tukey's multiple comparisons test was used to test for statistically significant differences between the three groups (n=3) (** P < 0.01; *** P < 0.001).*

Migration of the Crp127 epitope towards the surface of the capsule coincides with cell enlargement

To investigate the effect of small changes in cell size on Crp127 epitope distribution, we plotted cell body diameter against epitope proximity to the capsule surface for all cells measured (fig. 8A-B). Having done so, we noticed a correlation between the cell body diameter and epitope proximity to the capsule surface of yeast-like cells. In agreement with this, when plotting only cells with a cell body diameter between 5-10 μm, we found a positive correlation between cell body diameter and epitope proximity to the capsule surface in both strains tested (fig. 7F-G; H99 r = 0.65; Kn99α r = 0.66). Unlike cell body diameter, capsule diameter did not correlate with epitope proximity to the capsule surface, indicating that changes in capsule size do not explain changes in the proximity of the Crp127 to the capsule surface (fig. S4).

bioRxiv preprint doi: https://doi.org/10.1101/431650; this version posted October 1, 2018. The copyright holder for this preprint (which was not certified by peer review) is the author/funder. All rights reserved. No reuse allowed without permission.

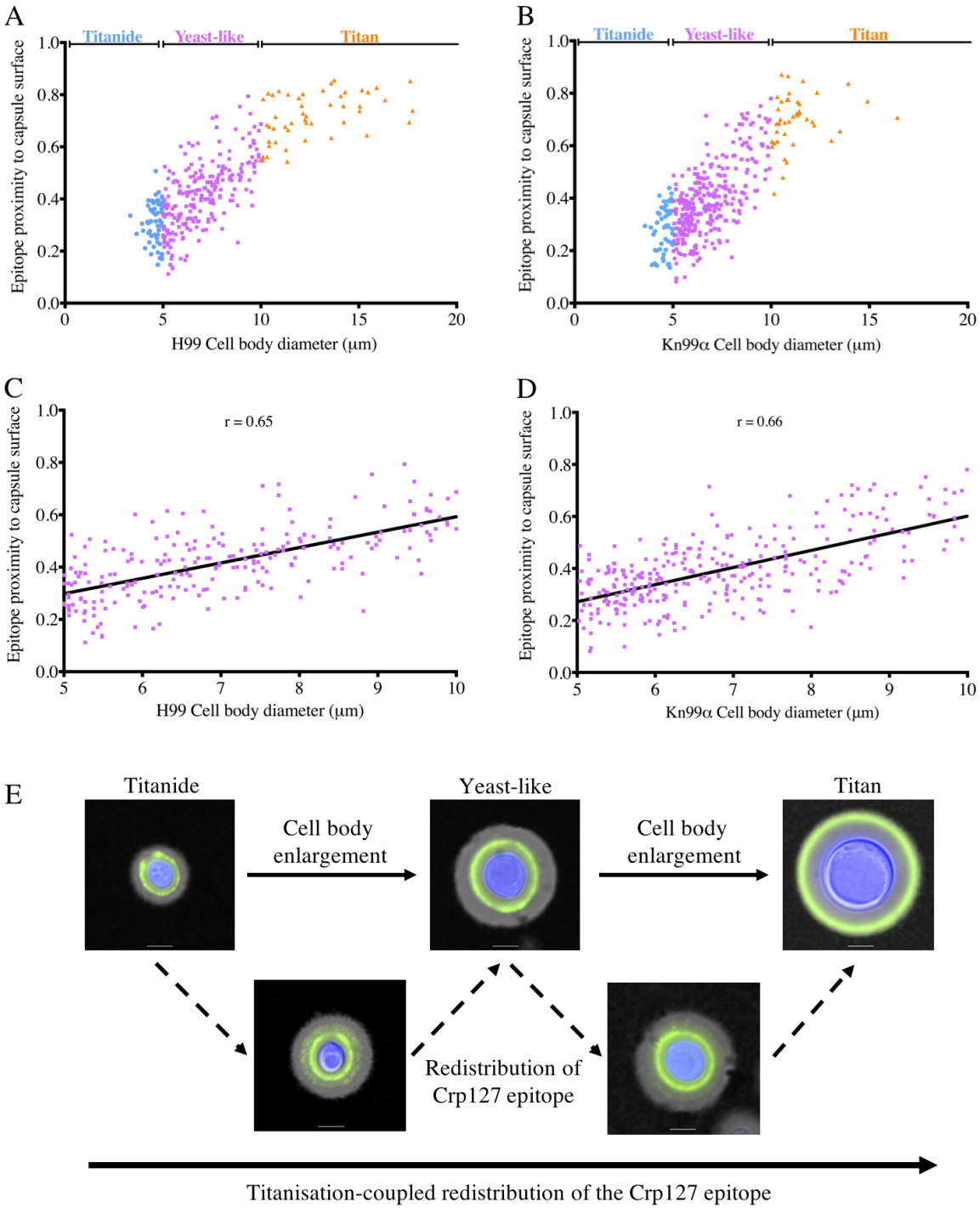

Fig. 8. Cell size positively correlates with proximity of the Crp127 epitope to the capsule surface and suggest a model of Titanisation-coupled epitope redistribution. *Cell body diameter was plotted against the epitope proximity to the capsule surface for all cells measured from strains* ***A)*** *H99 and* ***B)*** *Kn99α. Data points represent individual cells with cell body diameter <5 µm (blue circles), 5-10*

bioRxiv preprint doi: https://doi.org/10.1101/431650; this version posted October 1, 2018. The copyright holder for this preprint (which was not certified by peer review) is the author/funder. All rights reserved. No reuse allowed without permission.

519 *μm (purple squares) and >10 μm (orange triangles). Linear regression analysis of*
520 *cells with cell body diameter between 5-10 μm was used to assess the correlation*
521 *between cell size and Crp127 epitope proximity to the capsule surface for strains* ***C)***
522 *H99 and* ***D)*** *Kn99α.* ***E)*** *Positive correlation between the cell body diameter and*
523 *proximity of epitope to the capsule surface suggests a model by which Titanisation is*
524 *coupled to redistribution of the Crp127 epitope towards the capsule surface.*
525 *Representative images of Titanide, yeast-like and Titan cells exhibiting a typical*
526 *annular immunofluorescence binding pattern – in addition to Titanide and yeast-like*
527 *cells exhibiting a second more faint ring of antibody binding pattern outside of this –*
528 *are presented to propose a model by which epitope is added closer to the capsule*
529 *surface as cells enlarge. Images are merged for transmitted light, and Crp127*
530 *(green) and chitin (blue). Scale bars represent 5 μm.*
531
532 Our results suggest that the Crp127 epitope moves gradually to the capsule surface
533 as cells enlarge and age, raising the question of how this may occur. Throughout our
534 imaging experiments, the binding of Crp127 to the majority of Titanide and yeast-like
535 cells (in addition to all Titan cells) produced an annular immunofluorescence binding
536 pattern (fig. 8E). However, we also noticed that some Titanide and yeast-like cells
537 produced a second more faint ring of Crp127 epitope outside of this typical annular
538 ring (fig. 8E). This may represent the addition of Crp127 epitope closer to the
539 capsule surface, partially explaining how redistribution of this epitope coincides with
540 cell enlargement.
541
542 **Discussion**

bioRxiv preprint doi: https://doi.org/10.1101/431650; this version posted October 1, 2018. The copyright holder for this preprint (which was not certified by peer review) is the author/funder. All rights reserved. No reuse allowed without permission.

In this study, we demonstrated that a capsular epitope recognised by Crp127 – an anti-GXM mAb produced in our laboratory – contributes to serotype-specific differences in capsule structure. This epitope traverses the capsule as cells enlarge under conditions permissive for Titanisation, resulting in its differential distribution throughout the capsule of the three *C. neoformans* morphotypes found within Titanising populations. Detailing the accessibility and localisation of this epitope adds to the existing body of literature surrounding the variability of the cryptococcal capsule between strains and reveals yet another way in which Titan cell capsules are structurally distinct from those produced by yeast cells (21–23, 32, 40).

Based on our examination of a panel of mutants harbouring capsule defects, we propose that Crp127 is an anti-GXM mAb whose binding depends on GXM *O*-acetylation, but not xylosylation. When comparing sequences of the CDRs from Crp127 with four previously characterised anti-GXM IgM mAbs – namely 2D10, 12A1, 13F1 and 21D2 – we found that Crp127 CDRs were significantly different, particularly with regard to the light-chain variable (V_L) CDRs. These differences reflect differential gene usage and are likely to manifest as differences in epitope specificity (41, 42). In contrast, when we aligned the heavy-chain variable (V_H) and V_L sequences from Crp127 with those from anti-GXM IgG1 mAb 302, we noticed that the sequences were extremely similar as a result of identical variable region gene segment usage by these two mAbs. Identical gene segment usage is not entirely surprising given the restricted set of antibody gene segments utilised by antibodies specific to capsular polysaccharides (29), however the two mAbs were produced in response to GXM derived from different serotypes of *Cryptococcus*. Whereas mAb 302 was generated following the immunisation of a mouse with serotype D GXM

bioRxiv preprint doi: https://doi.org/10.1101/431650; this version posted October 1, 2018. The copyright holder for this preprint (which was not certified by peer review) is the author/funder. All rights reserved. No reuse allowed without permission.

(ATCC 24064) (43), we generated Crp127 through the immunisation of a mouse with a cocktail containing both serotype A (H99) and serotype B (R265) GXM. Whichever serotype of GXM activated the B cell from which Crp127 derives, the sequence similarities between mAbs Crp127 and 302 demonstrate that nearly identical antibodies can be elicited during infection by at least two different serotypes of *Cryptococcus*.

Crp127 binding shows strong serotype dependence, with serotype D strains being recognised most strongly, followed by serotype A strains. *C. gattii* serotype B strains show lower, heterogeneous Crp127 epitope recognition and a punctate immunofluorescence binding pattern, whilst serotype C strains entirely fail to bind the antibody. Interestingly, the predominant SRG found in GXM produced by serotype D, A, B and C contains 1, 2, 3 and 4 xylose substituents, respectively (15, 44). Together with the previous observation that β-(1,2)-xylose and *O*-acetyl groups are not added to the same backbone mannose residue (17, 36), this differential SRG usage may explain the variable Crp127 epitope recognition in one of two ways. For example, the additional xylose substituents present in the predominant SRG found in serotype B and C GXM may prevent addition of *O*-acetyl groups in such a way that the Crp127 epitope is not formed. Alternatively, the extra xylose substituents found in these SRGs may sterically hinder binding of Crp127 to its epitope. Studies that further elucidate the roles of specific proteins in GXM biosynthesis – together with advances in techniques that enable chemical synthesis of GXM oligosaccharides – will enhance our understanding of molecular how epitope recognition is achieved by anti-GXM mAbs like Crp127. Intriguingly, a recent transcriptomics study identified *CAS31* as being absent from the genome of strain CBS 10101, a serotype C isolate that we

bioRxiv preprint doi: https://doi.org/10.1101/431650; this version posted October 1, 2018. The copyright holder for this preprint (which was not certified by peer review) is the author/funder. All rights reserved. No reuse allowed without permission.

593 subsequently found was not recognised by Crp127. Whilst we cannot rule out the
594 possibility that other factors contribute to the inability of Crp127 to recognise
595 serotype C strains, it is tempting to speculate that the loss of *CAS31* function in this
596 lineage may explain its lack of reactivity with Crp127 (32, 34).
597
598 Perhaps our most striking observation regarding the Crp127 epitope was its
599 differential distribution throughout the capsules produced by Titanide, yeast-like and
600 Titan cells. No such differences have been consistently observed for other anti-GXM
601 mAbs E1, 2D10, 13F1 or 18B7 (7, 26), making this a unique feature of Crp127. The
602 positive correlation between cell size and Crp127 epitope proximity to the capsule
603 surface is suggestive of a scenario whereby the epitope in question is initially
604 produced in a capsular region adjacent to the cell wall in small Titanide cells, before
605 redistributing first to the midzone of yeast-like cells and eventually to the capsule
606 surface of Titan cells. This finding raises the intriguing question of how formation and
607 removal of the Crp127 epitope is so tightly spatially controlled within the capsule?
608 One possibility is that the epitope could be formed at the cell surface and then move
609 outwards as the capsular material elongates. Therefore, we speculate that since the
610 epitope moves outwards at a faster rate than the capsule expands, and since the
611 amount of epitope that initially surrounds a smaller Titanide or yeast-like cell would
612 not be sufficient to form the perimeter of capsule encasing a much larger Titan cell,
613 we instead favour a model in which the epitope is enzymatically removed and added
614 to different regions of the capsule during growth. For instance, it is possible that
615 GXM decorated with *O*-acetyl groups is added closer to the capsule surface in larger
616 cells or that such regions are “unmasked” in a different capsular region as the
617 capsule is reshaped during Titanisation (26). To summarise, our findings

bioRxiv preprint doi: https://doi.org/10.1101/431650; this version posted October 1, 2018. The copyright holder for this preprint (which was not certified by peer review) is the author/funder. All rights reserved. No reuse allowed without permission.

demonstrate that the differential distribution of specific epitopes within the cryptococcal capsule is yet another way in which Titan cells can be distinguished from canonical yeast cells, prompting further investigation into how redistribution of such epitopes occurs and what impact this has on the outcome of infection.

Materials and methods

Reagents, strains and mAbs

All reagents were purchased from Sigma-Aldrich unless stated otherwise. The *Cryptococcus* strains used in this study are described in table S1. The anti-GXM mAbs used in this study are described in table S2.

Growth of cryptococci

Cryptococcus strains were preserved at -80°C in MicroBank™ tubes (Thermo Fisher Scientific) prior to being stored on yeast extract peptone dextrose (YPD) agar plates at 4°C for a maximum of 30 days. Unless stated otherwise, strains were cultured on a rotary wheel at 20 rpm for 24 h at 25°C in round-bottom culture tubes containing 3 mL YPD broth. To induce capsule growth, *Cryptococcus* cells were grown in round-bottom culture tubes containing 3 mL Dulbecco's Modified Eagle's Media (DMEM) supplemented with 2 mM L-glutamine, 100 U/mL penicillin, 100 U/mL streptomycin and 10% foetal bovine serum (FBS) for 72 h in an incubator at 37°C and 200 rpm.

Hybridoma production and mAb purification

Cultures of *C. neoformans* H99 and *C. gattii* R265 were microfuged (4000 x *g* for 5 min) and washed three times in 1 mL Dulbecco's phosphate-buffered saline (PBS). Washed cultures were then heat killed for 60 minutes at 65°C. Following heat killing

bioRxiv preprint doi: https://doi.org/10.1101/431650; this version posted October 1, 2018. The copyright holder for this preprint (which was not certified by peer review) is the author/funder. All rights reserved. No reuse allowed without permission.

20 μL was plated onto YPD to confirm there were no viable cells. Heat-killed H99 and R265 cells were then either lysed (see below) or mixed 1:1 and stored at -20°C prior to inoculation. Fungal cells were lysed using Precellys tubes (UK05 03961-1-004) using programme 6400-2x10-005. Following lysis, lysis beads were microfuged (3000 x *g* for 1 min) and supernatant collected. H99 and R265 lysates were mixed 1:1 and stored at -20°C.

BALB/c mice were hyper-immunised with heat-killed H99 and R265 in addition to their lysates. Hybridomas were generated by a method that has previously been described (45). NS0 immortal fusion partner cells were fused with splenocytes mediated by polyethylene glycol (StemCell Technologies). All animal work was conducted in accordance with Home Office guidelines and following local ethical approval granted under animal licence 30/2788. Supernatants from clones were screened for reactivity with H99 and R265 cells using 96-well plates, with FITC-conjugated anti-mouse IgG and anti-mouse IgM antibodies used to identify positive clones via epifluorescence microscopy. Positive clone 127 was cultured in RPMI 1640 with IgG-depleted FBS and supernatant collected in a MiniPerm bioreactor (Sarstedt). MAb Crp127 was purified from supernatant using affinity chromatography and ProSep Thiosorb (Millipore).

Hybridoma sequencing and antibody sequence analysis

Sequencing of hybridomas was carried out by Absolute Antibody Ltd (UK). Sequencing was performed by whole transcriptome shotgun sequencing (RNA-Seq). In brief, hybridomas were cultured in Iscove's Modified Dulbecco's Media (IMDM) supplemented with 10% FBS in an incubator at 37°C and with 5% CO_2. Total RNA

bioRxiv preprint doi: https://doi.org/10.1101/431650; this version posted October 1, 2018. The copyright holder for this preprint (which was not certified by peer review) is the author/funder. All rights reserved. No reuse allowed without permission.

was extracted from cells and a barcoded cDNA library generated through RT-PCR using a random hexamer. Sequencing was performed using an Illumina HiSeq sequencer. Contigs were assembled and annotated for viable antibody sequences (i.e those not containing stop codons) to confirm the species and isotype of mAb Crp127 as murine and IgM, respectively.

Variable region gene usage was determined using VBASE2 software (46) and CDRs were predicted using the Kabat numbering system (47). Heavy-chain variable (V_H) and light-chain variable (V_L) sequences of mAb Crp127 were aligned with antibody sequences that have previously been described (35, 48). Amino acid sequences were aligned using Clustal Omega software (49) and annotated using ESpript software (50).

Immunolabelling

Cryptococcus cells were immunostained for flow cytometry and microscopy experiments. 1 mL of fungal culture was transferred to a 1.5 mL microcentrifuge tube, microfuged (15,000 x *g* for 1 min) and washed 3x in PBS. Cell density was determined using a haemocytometer and adjusted to 10^7 cells/mL in a final volume of 200 μL. 20 μg/mL Crp127, F12D2, 18B7 or mouse anti-human IgG (IgM isotype control) were added and samples mixed on a rotary wheel at 20 rpm for 1 h at room temperature. Untreated cells for use in flow cytometry were left untreated. After primary antibody treatment, samples were microfuged (15,000 x *g* for 1 min) and washed 3x in PBS to remove unbound primary antibody. 2 μg/mL Alexa-488-conjugated goat anti-mouse IgM (heavy chain) (Thermo Fisher Scientific), Alexa-647-conjugated goat anti-mouse IgM μ-chain (Abcam) or Alexa-647-conjugated

bioRxiv preprint doi: https://doi.org/10.1101/431650; this version posted October 1, 2018. The copyright holder for this preprint (which was not certified by peer review) is the author/funder. All rights reserved. No reuse allowed without permission.

F(ab')2-Goat anti-Mouse IgG (H+L) (Thermo Fisher Scientific) were added to antibody-treated samples and samples mixed on a rotary wheel at 20 rpm for 1 h at room temperature. Secondary antibody was also added to isotype control samples for flow cytometry. For microscopy experiments, 5 μg/mL calcofluor-white (CFW) was also added at this stage to label chitin. Following incubation with secondary antibody, samples were again microfuged (15,000 x *g* for 1 min) and washed 3x to remove unbound secondary antibody and CFW.

Flow cytometry

Flow cytometry experiments were performed with an Attune NxT Flow Cytometer equipped with an Attune Autosampler (Thermo Fisher Scientific). Untreated, isotype control and either Crp127 or 18B7 samples were prepared for each strain or conditions tested. Following immunostaining, samples were diluted to 5 x 10^6 cells/mL and 200 μL of *Cryptococcus* put into individual wells of a plastic round-bottom 96-well plate ready for insertion into the Attune Autosampler. Sample was collected from each well at a rate of 100 μL/min until 10,000 events were recorded. The 488 nm laser was used to detect primary antibody bound by Alexa-488-conjugated secondary antibodies, with the same voltage used to power the laser within each experiment. Flow cytometry data was then analysed using FlowJo (v10) software. Debris was excluded by using the FSC-A vs. SSC-A gating strategy, followed by exclusion of doublets using the FSC-A vs. FSC-H gating strategy (fig. S5). Where GXM-deficient mutants were analysed, samples were only gated to exclude debris due to the inseparable large aggregates formed by these mutants as a result of budding defects. After gating, histograms of fluorescence intensity were plotted and the median fluorescence intensity (MFI) determined. Corrected MFI

bioRxiv preprint doi: https://doi.org/10.1101/431650; this version posted October 1, 2018. The copyright holder for this preprint (which was not certified by peer review) is the author/funder. All rights reserved. No reuse allowed without permission.

values were calculated by subtracting the MFI value of the mAb-treated sample by the corresponding isotype control sample in the case of Crp127 or untreated sample where 18B7 was used. Across all experiments, MFI values returned from isotype control cells were extremely similar to those returned from untreated cells.

Confocal microscopy

Following the final washes of the immunostaining procedure, 2 μL of stained cryptococcal cells were spotted onto a glass slide and placed under a square glass coverslip. Where visualisation of the capsule was necessary, 2 μL Indian ink was also added to the glass slide. Imaging was performed on a Nikon A1R laser scanning confocal microscope using a 100x object lens and oil immersion. Alongside transmitted light, 639 nm and 405 nm lasers were used to detect Alexa-647-conjugated secondary antibodies and CFW, respectively. For cells with small capsules, Z-stacks spanning 8 μm were generated using steps of 0.27 μm. For capsule-induced cells, Z-stacks were taken across 20 μm using steps of 0.66 μm. Generation of maximum intensity projections (MIPs) and other image processing was performed using NIS-Elements and ImageJ software.

Chemical de-*O*-acetylation of capsular GXM

Where chemical de-*O*-acetylation of the capsule was required, cells were grown in YPD broth that had been adjusted pH 11 with NaOH and sterilised with a 0.22 μm filter. Round-bottom culture tubes containing 3 mL of pH 11 YPD broth was then placed on a rotary wheel turning at 20 rpm for 24 h at 25°C. This method was adapted from that used in a previous study (21).

bioRxiv preprint doi: https://doi.org/10.1101/431650; this version posted October 1, 2018. The copyright holder for this preprint (which was not certified by peer review) is the author/funder. All rights reserved. No reuse allowed without permission.

Phagocytosis assays

Phagocytosis assays were performed using the murine macrophage-like J774A.1 cell line (mouse BALB/cN; ATCC® TIB-67™). Cells were cultured in DMEM supplemented with 2 mM L-glutamine, 100 U/mL penicillin, 100 U/mL streptomycin and 10% FBS, before 1 x 10^5 cells were seeded onto round glass coverslips that had been placed into wells of a flat-bottom 24-well plate and incubated for 24 h at 37°C and 5% CO_2. Cells of strain R265 and Kn99α were opsonised with 18B7 or Crp127 as described for the first incubation of the immunostaining procedure. In the same way, cells were opsonised with 10% AB-human serum alone or in combination with Crp127. To achieve a multiplicity of infection (MOI) of 10, 10^6 R265 or Kn99α cells were then resuspended in serum-free DMEM and added to each well of J774A.1 cells. Following the infection, each well was gently washed 3x with 1 mL of warmed PBS to remove extracellular yeast. The contents of each well were then fixed with 4% paraformaldehyde prior to being washed a further 3x. Cover slips were then extracted from their well, any residual PBS removed by briefly submersing in sterile dH_2O and mounted onto glass slides with Prolong Gold Antifade Mountant (Thermo Fisher Scientific). The total number of internalised yeast cells per 100 J774A.1 cells (phagocytic index) was determined by microscopic examination using a Nikon TE2000-U microscope with a 60x objective lens and oil immersion.

Capsular swelling reactions

Capsule-induced cells were treated with 50 μg/mL Crp127 or 18B7 as described for the immunostaining procedure. 2 μL of *Cryptococcus* cells were then dropped onto a glass slide and placed under a square glass coverslip. Imaging was performed on the differential interference contrast (DIC) channel of a Nikon TE2000-U microscope

bioRxiv preprint doi: https://doi.org/10.1101/431650; this version posted October 1, 2018. The copyright holder for this preprint (which was not certified by peer review) is the author/funder. All rights reserved. No reuse allowed without permission.

using a 60x objective lens with oil immersion. Image processing was performed using NIS-Elements and ImageJ software.

Titan cell experiments

Titan cells that exhibit all the properties of *in vivo* Titan cells were induced *in vitro* using a previously described protocol (9). *C. neoformans* H99 and Kn99α cells were cultured in glass conical flasks containing 10 mL yeast nitrogen base (YNB) + 2% glucose at 30°C and 200 rpm for 24 h. Cells were adjusted to an OD_{600} reading of 0.001 before being transferred into 10% heat-inactivated foetal calf serum (HI-FCS) at a final volume of 3 mL in a plastic six-well plate and grown for 72 h at 37°C and 5% CO_2. To begin a culture derived solely from Titan cells, cells were passed through an 11 μm filter, trapping only larger cells on the filter paper. This filter paper was then washed in PBS to re-suspend Titan cells. Between 10^3 and 10^4 Titan cells were then transferred into 3 mL HI-FCS in a plastic six-well plate and cultured for a further 72 h at 37°C and 5% CO_2. Titanising populations were prepared for imaging according to the method described for immunostaining. Imaging was performed on a Nikon TE2000-U microscope using a 60x objective lens with oil immersion.

To quantify the proximity of the Crp127 epitope to the capsule surface was quantified, ImageJ software was used to draw regions of interest (ROIs) around the cell body, the immunofluorescence binding pattern of the Crp127 and the capsule surface (as determined by Indian ink staining). For each cell measured, the area of these three ROIs was determined before the area of the cell body was subtracted from the areas calculated for both the Crp127 epitope ROI and the capsule surface ROI. Finally, the area of the Crp127 epitope ROI was divided by the capsule surface

bioRxiv preprint doi: https://doi.org/10.1101/431650; this version posted October 1, 2018. The copyright holder for this preprint (which was not certified by peer review) is the author/funder. All rights reserved. No reuse allowed without permission.

ROI as a means of quantifying the proximity of the Crp127 epitope to the capsule surface. A mean number of 111 and 133 cells were measured per biological replicate for strain H99 and Kn99α, respectively. Image processing was performed using NIS-Elements software.

Experimental design and statistical analysis

For each experiment described, three biological repeats were performed as independent experiments that were carried out on different days. All datasets were analysed using GraphPad Prism 7 software.

Acknowledgements

Provision of antibodies, strains and assistance

We gratefully acknowledge our colleagues Tamara Doering (Washington University), Guilhem Janbon (Institut Pasteur), Arturo Casadevall (Johns Hopkins) and Thomas Kozel (University of Nevada) providing antibodies and strains and for their invaluable advice regarding this project. We are also grateful to Alessandro Di Maio, Leanne Taylor-Smith and Joao Correia (University of Birmingham) for assistance with confocal microscopy and subsequent image processing.

Author contributions

Experiments were designed and conducted by MP, XZ and EB. The Crp127 antibody was raised and initially characterised by SAJ and MG. ERB and RCM helped design and oversee this project. Data figures and text were prepared by MP and then edited and revised by all the other authors.

bioRxiv preprint doi: https://doi.org/10.1101/431650; this version posted October 1, 2018. The copyright holder for this preprint (which was not certified by peer review) is the author/funder. All rights reserved. No reuse allowed without permission.

Competing interests

The authors declare no competing interests with this work.

Funding

This work was made possible via funding from the Lister Institute for Preventive Medicine and the European Research Council under the European Union's Seventh Framework Programme (FP/2007-2013)/ERC Grant Agreement No. 614562 and from the Biotechnology and Biological Sciences Research Council (BBSRC) via grant BB/R008485/1. RCM is additionally supported by a Wolfson Royal Society Research Merit Award. ERB was supported by the UK Biotechnology and Biological Research Council (http://www.bbsrc.ac.ukhttp://www.bbsrc.ac.uk; BB/M014525/1).

Data and materials availability: All data needed to evaluate the conclusions drawn in this paper are present in the paper and/or the supplementary materials. Additional data related to this paper may be requested from the authors. The Crp127 antibody described here is available via Ximbio.com.

References

1. Rajasingham R, Smith RM, Park BJ, Jarvis JN, Govender NP, Chiller TM, Denning DW, Loyse A, Boulware DR. 2017. Global burden of disease of HIV-associated cryptococcal meningitis: an updated analysis. Lancet Infect Dis 17:873–881.
2. MacDougall L, Fyfe M, Romney M, Starr M, Galanis E. 2011. Risk Factors for *Cryptococcus gattii* Infection, British Columbia, Canada. Emerg Infect Dis 17:193–199.
3. Galanis E, Macdougall L, Kidd S, Morshed M, British Columbia Cryptococcus

bioRxiv preprint doi: https://doi.org/10.1101/431650; this version posted October 1, 2018. The copyright holder for this preprint (which was not certified by peer review) is the author/funder. All rights reserved. No reuse allowed without permission.

gattii Working Group the BCC gattii W. 2010. Epidemiology of Cryptococcus gattii, British Columbia, Canada, 1999-2007. Emerg Infect Dis 16:251–7.

4. Harris JR, Lockhart SR, Debess E, Marsden-Haug N, Goldoft M, Wohrle R, Lee S, Smelser C, Park B, Chiller T. 2011. Cryptococcus gattii in the United States: Clinical Aspects of Infection With an Emerging Pathogen. Clin Infect Dis 53:1188–1195.

5. Granger DL, Perfect JR, Durack DT. 1985. Virulence of Cryptococcus neoformans. Regulation of capsule synthesis by carbon dioxide. J Clin Invest 76:508–16.

6. Fromtling RA, Shadomy HJ, Jacobson ES. 1982. Decreased virulence in stable, acapsular mutants of cryptococcus neoformans. Mycopathologia 79:23–9.

7. Zaragoza O, García-Rodas R, Nosanchuk JD, Cuenca-Estrella M, Rodríguez-Tudela JL, Casadevall A. 2010. Fungal Cell Gigantism during Mammalian Infection. PLoS Pathog 6:e1000945.

8. Okagaki LH, Strain AK, Nielsen JN, Charlier C, Baltes NJ, Chrétien F, Heitman J, Dromer F, Nielsen K. 2010. Cryptococcal Cell Morphology Affects Host Cell Interactions and Pathogenicity. PLoS Pathog 6:e1000953.

9. Dambuza IM, Drake T, Chapuis A, Zhou X, Correia J, Taylor-Smith L, LeGrave N, Rasmussen T, Fisher MC, Bicanic T, Harrison TS, Jaspars M, May RC, Brown GD, Yuecel R, MacCallum DM, Ballou ER. 2018. The Cryptococcus neoformans Titan cell is an inducible and regulated morphotype underlying pathogenesis. PLOS Pathog 14:e1006978.

10. Okagaki LH, Nielsen K. 2012. Titan cells confer protection from phagocytosis in Cryptococcus neoformans infections. Eukaryot Cell 11:820–6.

bioRxiv preprint doi: https://doi.org/10.1101/431650; this version posted October 1, 2018. The copyright holder for this preprint (which was not certified by peer review) is the author/funder. All rights reserved. No reuse allowed without permission.

870 11. Crabtree JN, Okagaki LH, Wiesner DL, Strain AK, Nielsen JN, Nielsen K.
871 2012. Titan cell production enhances the virulence of Cryptococcus
872 neoformans. Infect Immun 80:3776–85.
873 12. Carter DA, Fernandes KE, Brockway A, Haverkamp M, Cuomo CA, Ogtrop F
874 Van, Perfect JR. 2018. Phenotypic variability correlates with clinical outcome in
875 Cryptococcus isolates obtained from Botswanan HIV/AIDS patients. bioRxiv
876 418897.
877 13. Zhou X, Ballou ER. 2018. The Cryptococcus neoformans Titan Cell: From In
878 Vivo Phenomenon to In Vitro Model. Curr Clin Microbiol Reports 1–9.
879 14. Casadevall A, Coelho C, Cordero RJB, Dragotakes Q, Jung E, Vij R, Wear
880 MP. 2018. The Capsule of Cryptococcus neoformans.
881 https://doi.org/101080/21505594201814310 87.
882 15. Cherniak R, Valafar H, Morris LC, Valafar F. 1998. Cryptococcus neoformans
883 chemotyping by quantitative analysis of 1H nuclear magnetic resonance
884 spectra of glucuronoxylomannans with a computer-simulated artificial neural
885 network. Clin Diagn Lab Immunol 5:146–59.
886 16. Cherniak R, Reiss E, Slodki ME, Plattner RD, Blumer SO. 1980. Structure and
887 antigenic activity of the capsular polysaccharide of Cryptococcus neoformans
888 serotype A. Mol Immunol 17:1025–1032.
889 17. Janbon G, Himmelreich U, Moyrand F, Improvisi L, Dromer F. 2001. Cas1p is
890 a membrane protein necessary for the O-acetylation of the Cryptococcus
891 neoformans capsular polysaccharide. Mol Microbiol 42:453–67.
892 18. Dromer F, Gueho E, Ronin O, Dupont B. 1993. Serotyping of Cryptococcus
893 neoformans by using a monoclonal antibody specific for capsular
894 polysaccharide. J Clin Microbiol 31:359–63.

bioRxiv preprint doi: https://doi.org/10.1101/431650; this version posted October 1, 2018. The copyright holder for this preprint (which was not certified by peer review) is the author/funder. All rights reserved. No reuse allowed without permission.

19. McFadden DC, Fries BC, Wang F, Casadevall A. 2007. Capsule Structural Heterogeneity and Antigenic Variation in Cryptococcus neoformans. Eukaryot Cell 6:1464–1473.

20. McFadden D, Zaragoza O, Casadevall A. 2006. The capsular dynamics of Cryptococcus neoformans. Trends Microbiol 14:497–505.

21. Gates-Hollingsworth MA, Kozel TR. 2009. Phenotypic heterogeneity in expression of epitopes in the Cryptococcus neoformans capsule. Mol Microbiol 74:126–138.

22. Franzot SP, Mukherjee J, Cherniak R, Chen LC, Hamdan JS, Casadevall A. 1998. Microevolution of a standard strain of Cryptococcus neoformans resulting in differences in virulence and other phenotypes. Infect Immun 66:89–97.

23. Rivera J, Feldmesser M, Cammer M, Casadevall A. 1998. Organ-dependent variation of capsule thickness in Cryptococcus neoformans during experimental murine infection. Infect Immun 66:5027–30.

24. Charlier C, Chrétien F, Baudrimont M, Mordelet E, Lortholary O, Dromer F. 2005. Capsule structure changes associated with Cryptococcus neoformans crossing of the blood-brain barrier. Am J Pathol 166:421–32.

25. Garcia-Hermoso D, Dromer F, Janbon G. 2004. Cryptococcus neoformans Capsule Structure Evolution In Vitro and during Murine Infection. Infect Immun 72:3359–3365.

26. Mukaremera L, Lee KK, Wagener J, Wiesner DL, Gow NAR, Nielsen K. 2018. Titan cell production in Cryptococcus neoformans reshapes the cell wall and capsule composition during infection. Cell Surf 1:15–24.

27. Wiesner DL, Specht CA, Lee CK, Smith KD, Mukaremera L, Lee ST, Lee CG,

bioRxiv preprint doi: https://doi.org/10.1101/431650; this version posted October 1, 2018. The copyright holder for this preprint (which was not certified by peer review) is the author/funder. All rights reserved. No reuse allowed without permission.

Elias JA, Nielsen JN, Boulware DR, Bohjanen PR, Jenkins MK, Levitz SM, Nielsen K. 2015. Chitin recognition via chitotriosidase promotes pathologic type-2 helper T cell responses to cryptococcal infection. PLoS Pathog 11:e1004701.

28. Houpt DC, Pfrommer GS, Young BJ, Larson TA, Kozel TR. 1994. Occurrences, immunoglobulin classes, and biological activities of antibodies in normal human serum that are reactive with Cryptococcus neoformans glucuronoxylomannan. Infect Immun 62:2857–64.

29. Rohatgi S, Pirofski L-A. 2015. Host immunity to Cryptococcus neoformans. Future Microbiol 10:565–81.

30. Kozel TR, Levitz SM, Dromer F, Gates MA, Thorkildson P, Janbon G. 2003. Antigenic and biological characteristics of mutant strains of Cryptococcus neoformans lacking capsular O acetylation or xylosyl side chains. Infect Immun 71:2868–75.

31. Moyrand F, Klaproth B, Himmelreich U, Dromer F, Janbon G. 2002. Isolation and characterization of capsule structure mutant strains of Cryptococcus neoformans. Mol Microbiol 45:837–849.

32. Cleare W, Cherniak R, Casadevall A. 1999. In vitro and in vivo stability a Cryptococcus neoformans glucuronoxylomannan epitope that elicits protective antibodies. Infect Immun 67:3096–3107.

33. Ellerbroek PM, Lefeber DJ, van Veghel R, Scharringa J, Brouwer E, Gerwig GJ, Janbon G, Hoepelman AIM, Coenjaerts FEJ. 2004. O-acetylation of cryptococcal capsular glucuronoxylomannan is essential for interference with neutrophil migration. J Immunol 173:7513–20.

34. Urai M, Kaneko Y, Ueno K, Okubo Y, Aizawa T, Fukazawa H, Sugita T, Ohno

bioRxiv preprint doi: https://doi.org/10.1101/431650; this version posted October 1, 2018. The copyright holder for this preprint (which was not certified by peer review) is the author/funder. All rights reserved. No reuse allowed without permission.

945 H, Shibuya K, Kinjo Y, Miyazaki Y. 2015. Evasion of Innate Immune
946 Responses by the Highly Virulent Cryptococcus gattii by Altering Capsule
947 Glucuronoxylomannan Structure. Front Cell Infect Microbiol 5:101.
948 35. Casadevall A, DeShaw M, Fan M, Dromer F, Kozel TR, Pirofski LA. 1994.
949 Molecular and idiotypic analysis of antibodies to Cryptococcus neoformans
950 glucuronoxylomannan. Infect Immun 62:3864–72.
951 36. Moyrand F, Chang YC, Himmelreich U, Kwon-Chung KJ, Janbon G. 2004.
952 Cas3p belongs to a seven-member family of capsule structure designer
953 proteins. Eukaryot Cell 3:1513–24.
954 37. Hagen F, Khayhan K, Theelen B, Kolecka A, Polacheck I, Sionov E, Falk R,
955 Parnmen S, Lumbsch HT, Boekhout T. 2015. Recognition of seven species in
956 the Cryptococcus gattii/Cryptococcus neoformans species complex. Fungal
957 Genet Biol 78:16–48.
958 38. Mukherjee J, Cleare W, Casadevall A. 1995. Monoclonal antibody mediated
959 capsular reactions (Quellung) in Cryptococcus neoformans. J Immunol
960 Methods 184:139–43.
961 39. Hommel B, Mukaremera L, Cordero RJB, Coelho C, Desjardins CA, Sturny-
962 Leclère A, Janbon G, Perfect JR, Fraser JA, Casadevall A, Cuomo CA,
963 Dromer F, Nielsen K, Alanio A. 2018. Titan cells formation in Cryptococcus
964 neoformans is finely tuned by environmental conditions and modulated by
965 positive and negative genetic regulators. PLOS Pathog 14:e1006982.
966 40. Fries BC, Taborda CP, Serfass E, Casadevall A. 2001. Phenotypic switching
967 of Cryptococcus neoformans occurs in vivo and influences the outcome of
968 infection. J Clin Invest 108:1639–48.
969 41. Mukherjee J, Scharff MD, Casadevall A. 1992. Protective murine monoclonal

bioRxiv preprint doi: https://doi.org/10.1101/431650; this version posted October 1, 2018. The copyright holder for this preprint (which was not certified by peer review) is the author/funder. All rights reserved. No reuse allowed without permission.

970 antibodies to Cryptococcus neoformans. Infect Immun 60:4534–41.
971 42. Casadevall A, Mukherjee J, Devi SJ, Schneerson R, Robbins JB, Scharff MD.
972 1992. Antibodies elicited by a Cryptococcus neoformans-tetanus toxoid
973 conjugate vaccine have the same specificity as those elicited in infection. J
974 Infect Dis 165:1086–93.
975 43. Eckert TF, Kozel TR. 1987. Production and characterization of monoclonal
976 antibodies specific for Cryptococcus neoformans capsular polysaccharide.
977 Infect Immun 55:1895–9.
978 44. Janbon G. 2004. Cryptococcus neoformans capsule biosynthesis and
979 regulation. FEMS Yeast Res 4:765–771.
980 45. Galfrè G, Milstein C. 1981. [1] Preparation of monoclonal antibodies:
981 Strategies and procedures. Methods Enzymol 73:3–46.
982 46. Retter I, Althaus HH, Münch R, Müller W. 2004. VBASE2, an integrative V
983 gene database. Nucleic Acids Res 33:D671–D674.
984 47. Wu TT, Kabat EA. 1970. An analysis of the sequences of the variable regions
985 of Bence Jones proteins and myeloma light chains and their implications for
986 antibody complementarity. J Exp Med 132:211–50.
987 48. Nakouzi A, Valadon P, Nosanchuk J, Green N, Casadevall A. 2001. Molecular
988 basis for immunoglobulin M specificity to epitopes in Cryptococcus neoformans
989 polysaccharide that elicit protective and nonprotective antibodies. Infect Immun
990 69:3398–409.
991 49. McWilliam H, Li W, Uludag M, Squizzato S, Park YM, Buso N, Cowley AP,
992 Lopez R. 2013. Analysis Tool Web Services from the EMBL-EBI. Nucleic Acids
993 Res 41:W597–W600.
994 50. Robert X, Gouet P. 2014. Deciphering key features in protein structures with

bioRxiv preprint doi: https://doi.org/10.1101/431650; this version posted October 1, 2018. The copyright holder for this preprint (which was not certified by peer review) is the author/funder. All rights reserved. No reuse allowed without permission.

995 the new ENDscript server. Nucleic Acids Res 42:W320–W324.

996